NANO LETTERS

2006
Vol. 6, No. 9
2021−2025

Nanoscale Patterning on Insulating Substrates by Critical Energy Electron Beam Lithography

Jaebum Joo, Brian Y. Chow, and Joseph M. Jacobson*

The Center for Bits and Atoms, MIT Media Laboratory, Massachusetts Institute of Technology, 20 Ames Street, Cambridge, Massachusetts 02139

Received May 28, 2006; Revised Manuscript Received July 17, 2006

ABSTRACT

This Letter describes a method to generate nanometer scale patterns on insulating substrates and wide band gap materials using critical energy electron beam lithography. By operating at the critical energy (E_2) where a charge balance between incoming and outgoing electrons leaves the surface neutral, charge-induced pattern distortions typically seen in e-beam lithography on insulators were practically eliminated. This removes the need for conductive dissipation layers or differentially pumped e-beam columns with sophisticated gas delivery systems to control charging effects. Using a "scan square" method to find the critical energy, sub-100 nm features in 65 nm thick poly(methyl methacrylate) on glass were achieved at area doses as low as 10 μC/cm^2 at $E_2 = 1.3$ keV. This method has potential applications in high-density biochips, flexible electronics, and optoelectronics and may improve the fidelity of low voltage e-beam lithography for parallel microcolumn arrays.

Electron beam (e-beam) lithography is a powerful tool for nanoscale fabrication, but its applicability to insulating substrates is often limited because of surface charging effects. Unlike patterning on conducting substrates that dissipate excess charge as the beam passes through the resist, charge is trapped near the surface when the substrate is insulating. This charging causes an unbalanced surface potential of the resist[1−5] that deflects the beam and causes severe pattern distortion.[6−10] Several methods have been employed to prevent the pattern distortion, most commonly the use of a conductive layer above the resist[11−13] that requires additional processing steps and the use of conducting polymers as the resist itself.[14−16] A third approach, known as environmental scanning electron microscopy (ESEM), delivers gas molecules into the chamber that are ionized upon e-beam impact and neutralize surface charging,[17−21] but it requires a differentially pumped electron beam column and a sophisticated gas delivery system.

In this Letter, we describe a method to fabricate nanostructures on insulating substrates using conventional e-beam lithography tools and resists, which we have termed critical energy electron beam lithography (CE-EBL). In an e-beam system, the total electron yield ($\sigma = \delta + \eta$), which is the sum of the secondary electron (SE) yield (δ) and the backscattered electron (BSE) yield (η), changes as a function of the accelerating voltage. It is intuitive that at high accelerating voltages, an e-beam negatively charges insulators ($\sigma < 1$), but less commonly known is that at low beam energies, the surface can actually be charged positive ($\sigma > 1$) when more electrons are scattered or ejected from the surface than are stored in the insulator itself. At the critical beam energy, σ equals unity, and a charge balance between incoming and outgoing electrons is satisfied even though the substrate is not conducting. As a result, controlling the beam energy alone can minimize surface charging and pattern distortion. We adapted a concept of low voltage scanning electron microscopy (LVSEM) to find this charge neutral condition[2,4,22] of the resist-on-insulator to practically eliminate pattern distortion without charge dissipation layers or variable pressure control of the system. A similar method has been used to control pattern distortion in the formation of silicides on semiconductors[23] for low-voltage electron beam lithography (LVEBL),[24−26] and here the technique is extended to patterning resists on insulators.

Figure 1 shows the general characteristics of the total electron yield of polymers irradiated at different e-beam energies. The current balance equation for conducting materials in an e-beam system is given by[4]

$$I_B = \delta I_B + \eta I_B + I_{SC} \quad (1)$$

where I_B is the beam current and I_{SC} is the current flowing from substrate to ground or leakage current. If the substrate is fully insulating, $I_{SC} = 0$, and the excess charge buildup (ΔQ) in the substrate is

$$\Delta Q/s = (1 - \sigma) I_B \quad (2)$$

* Corresponding author. E-mail: jacobson@media.mit.edu.

10.1021/nl061211q CCC: $33.50
Published on Web 07/28/2006

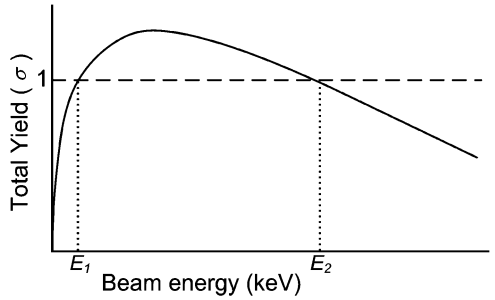

Figure 1. Total electron yield (σ) vs beam energy for a typical resist. The bulk insulating material is positive charged when $\sigma > 1$ and negatively charged when $\sigma < 1$. The charge buildup is zero at the critical energy or crossover voltage (E_1, E_2), where σ is unity.

If the beam energy (E) is larger than a critical energy or crossover voltage, E_2, then $\sigma < 1$, and the specimen becomes negatively charged. The specimen will be positively charged ($\sigma > 1$) when the beam energy is between two critical energies, E_1 and E_2. Because it is impractical to consider E_1, which is not within the range of electron lithography systems ($E_1 \sim 10-100$ eV for insulators), the specimen will be considered positively charged when $E < E_2$ throughout this Letter. The charging (ΔQ) is minimized if we pattern at the critical beam energy, E_2, where $\sigma = 1$.

While eqs 1 and 2 are steady-state equations for large area flood exposure (i.e., imaging), electron beam patterning is a dynamic process that utilizes a focused beam, and thus, the above description is somewhat simple. However, since the surface is neutral before and after irradiation when patterned at E_2 and the leakage current is effectively zero (in the time scale the beam dwells per spot), the equations are reasonable first-order approximations. On the other hand, when charge builds up during patterning ($E \neq E_2$), the time variation of the surface potential must be considered, a complete analytical description for which is provided by Gong and coworkers.[5]

Using a variable magnification scanning method or "scan square",[4,27] the critical beam energy (E_2) was found to be 1.3 keV for 65 nm poly(methyl methacrylate) (950K PMMA A2, Microchem) on glass (Electron Microscopy Slides) or 1 μm thermal oxide (Wafernet). For all results reported in this Letter, PMMA was spin-coated for 40 s at 5000 rpm, prebaked at 170 °C for 30 min, and developed with 1:3 methyl isobutyl ketone/2-propanol (MIBK/IPA) for 60 s. In the scan square experiment, the microscope (FEI-XL30 ESEM equipped with a Nabity control system operated in standard high-vacuum mode) was first set at low magnification ($\times$200) in live image mode for 10 s, and then the magnification was raised ($\times$500) for 5 s. The final voltage contrast SEM images (Figure 2) were captured after dropping back to the original magnification. In Figure 2a where E(0.5 keV) $< E_2$, the high magnification region (inner part of the image) was positively charged. The region appears dark because it re-collects its own SE emission and because the decreased electric field between the region and the SE detector lowers the detector efficiency. In Figure 2b, the system was operated at the critical beam energy, E_2(1.3 keV), and there was virtually no contrast difference between the inner and outer regions. In Figure 2c, where E(2.0 keV) $> E_2$, the high magnification region was negatively charged and appears bright because of electron repulsion from the surface and increased SE detector efficiency. Scan square experiments were performed at several spots across the substrate and at various chamber pressures from 9.7×10^{-3} to 3.0×10^{-5} Torr. While scan squares can vary due to factors such as chamber pressure, surface adsorbates, and stage tilt, the values for E_2 were consistent within the control limits over the acceleration voltage of the commercial lithography system ($\pm$0.1 keV). Although E_2 did not vary throughout the experiments, a scan square measurement was made on every substrate prior to patterning to account for possible variations.

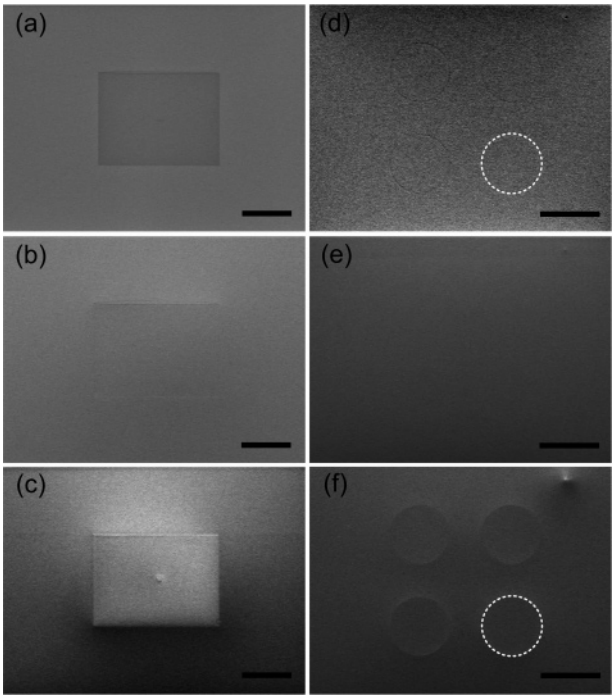

Figure 2. (a−c) "Scan square" or variable magnification SEM images after dropping the magnification from $\times$500 to $\times$200 operating at (a) 0.5 keV, (b) 1.3 keV, and (c) 2.0 keV in order to find the critical energy (E_2) of 65 nm PMMA on glass. The dark rectangles represent positively charged high-magnification regions, and the bright rectangles represent negatively charged regions. Virtually no voltage contrast exists at the critical energy, $E_2 = 1.3$ keV. Scale bar = 200 μm. (d−f) Images of a 2 $\times$ 2 array of circular charge patterns written at (d) 1.2 keV, (e) 1.3 keV, and (f) 1.4 keV show that the E_2 value during steady-state imaging conditions is equal to the value during dynamic patterning conditions within the control limits of the lithography system ($\pm$0.1 keV). Dotted lines highlight the bottom right circle of the array. Scale bar = 100 μm.

To test that the critical voltage measured from the flood exposure of a scan square is equal to the critical voltage for a tightly focused beam used in patterning, circular charge patterns were written at 1.2, 1.3, and 1.4 keV ($E_2 \pm 0.1$ keV) as shown in parts d−f of Figure 2. Both the positive and negative charge patterns created at 1.2 and 1.4 keV, respectively, were observable while no charge pattern could be seen when patterned at 1.3 keV. Therefore, within the control limits of the system, the critical voltages during scan squares and patterning were equal.

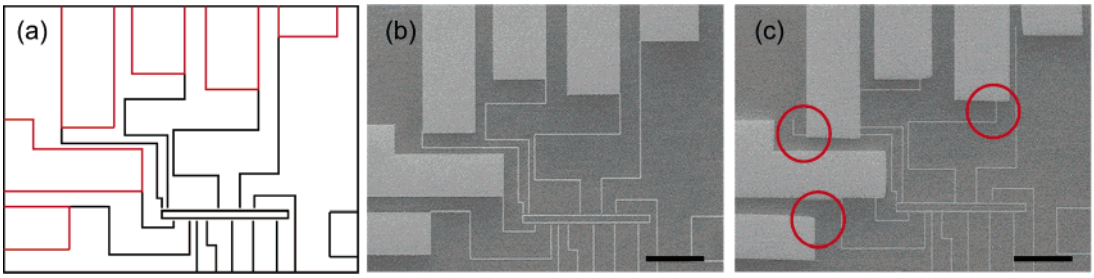

Figure 3. Pattern distortion in electron beam lithography on insulators as a result of surface charging. (a) Design of the desired pattern. SEM images of 10 nm thick Au electrodes on glass after lift-off of PMMA patterned at (b) 1.3 keV (E_2) and (c) 5 keV. Charge induced pattern distortions are prominent at 5 keV (circled). Scale bar = 10 μm.

The pattern distortion generated by surface charging on glass is demonstrated in Figure 3, which shows 10 nm thick thermally evaporated gold (Edwards FL-400) patterns after PMMA lift-off with acetone. There was no apparent distortion between the desired pattern and the metal structures at E_2 (parts a and b of Figure 3). However, line mismatches (circled in Figure 3c) were observed when the beam energy was 5 keV because the beam was deflected by the negative surface charge. Since both patterns were created at the critical dose at 5 keV (30 μC/cm^2), the deflection was a result of the different accelerating voltages and not the charge per unit area.

The pattern deflection was quantified by a method previously reported by Craighead and co-workers.[6] Briefly, two single-pass reference lines spaced 1 μm apart were first patterned at various beam energies: 0.6, 1.3, 2.0, and 5.0 keV (at doses of 0.1, 0.125, 0.4, 0.1 nC/cm, respectively). Large charge pads (10, 20, and 30 μm) were then patterned with a 30 μC/cm^2 area dose for all beam energies, and finally, a third single-pass line was patterned between the charge pad and the reference lines. The line doses for beam energies E_2 and above were the critical doses for exposure, but since there is no critical dose at 0.6 keV because of beam penetration depth issues, the dose at 0.6 keV was chosen arbitrarily to be smaller than the dose at E_2 = 1.3 keV. While these line doses vary slightly, the main source of pattern distortion should be the charge pad. After the resist was developed and a thin 5 nm Au film was thermally evaporated, the samples were imaged to determine the average deflection. Metal lift-off was not performed because the 0.6 keV beam could not fully expose the resist.

As can be seen in Figure 4, there were very large beam deflections at all beam energies except E_2. The deflection at 0.6 keV is of particular note because it represents distortion from positive surface charging, which is not typically considered in electron beam patterning but may factor into low-voltage electron beam lithography systems. The amounts of charging and beam deflection depend on a variety of factors, such as the acceleration voltage, the electron yield at specific beam energies (σ), and e-beam induced conductivity.[28] The average deflection for the sample patterned at E_2 was very small, measuring 12 nm for the 10 μm charge pad. If one assumes that the uncertainty is ~10 nm due to edge roughness, pixel size, and the lithography system itself,[6] this test shows that CE-EBL can nearly eliminate pattern distortion on insulators. However, charging effects are not totally eliminated by operating at E_2 because the line deflection increased slightly to ~20 nm with the larger charge pads, although systems with finer control over the acceleration voltage may be capable of completely eliminating pattern distortion.

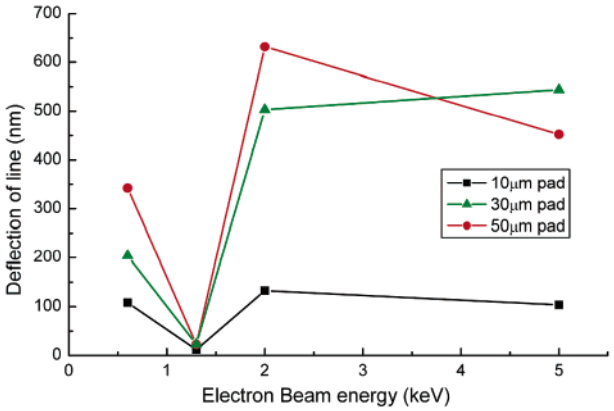

Figure 4. Line deflection at various voltages based on methods reported by Craighead and co-workers.[6] Two parallel single-pass reference lines were first patterned with a 1 μm gap, followed by charge pads written at 30 μC/cm^2. Finally, a third single-pass line was patterned between the pad and the reference line. 5 nm Au was evaporated after developing the PMMA and imaged under SEM to determine the line deflection. The deflection was virtually eliminated at E_2 = 1.3 keV, whereas the beam was largely deflected due to positive surface charging below E_2 and negative charging above it.

Figure 5 shows contact mode atomic force microscopy (AFM) images of postdeveloped PMMA on glass (Digital Instruments 3000, Veeco DNP-S tips). The resist was uniformly exposed as evident by the flat wells in the line section profile shown in Figure 5c. Such line section profiles were used to determine the critical area dose to expose the 65 nm PMMA film on glass, which was measured to be 10 μC/cm^2 (Figure 6), and the critical line dose was found to be 0.125 nC/cm. These values are over an order of magnitude lower than typical PMMA doses at high beam energies. Given such low critical dose values, which are common to low-energy electron beam lithography methods[25] because the energy per unit volume scales as ~1/E^4, CE-EBL is well suited for prototyping nanostructures, especially considering that the process eliminates the deposition and etching of charge dissipation layers. The smallest feature size obtained when patterned with an area dose of 10 μC/cm^2 was 60 nm (Figure 7), which is approximately the theoretical limit for

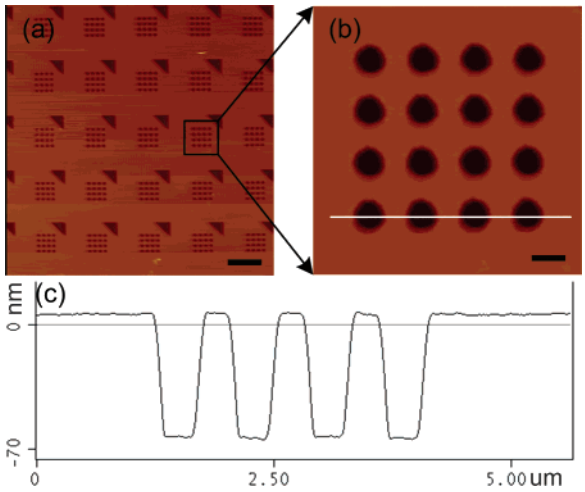

Figure 5. AFM topography image of developed PMMA on glass generated by CE-EBL. (a) Scale bar = 5 μm. (b) Scale bar = 500 nm. (c) The flat wells in the line section indicate that the exposure is uniform.

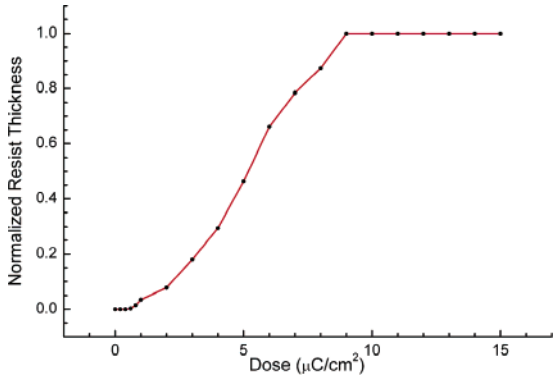

Figure 6. Penetration depth measurements taken from AFM line sections of developed PMMA show that the area dose for full exposure was 10 μC/cm^2 for a resist of 65 nm thickness.

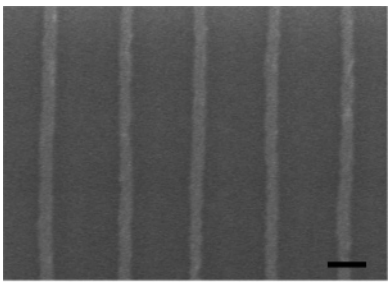

Figure 7. Line test SEM images of 5 nm thick Au after lift-off. The minimum feature size was ~60 nm when patterned with an area dose of 10 μC/cm^2. Scale bar = 100 nm.

this particular resist thickness due to lateral scattering based on Monte Carlo simulations (CASINO v2.0).[29] Like most low-voltage e-beam techniques, the patterning resolution of CE-EBL is limited by lateral scattering, but smaller feature sizes may be attainable with thinner PMMA films or different resists.

To demonstrate one potential application of CE-EBL, we created binary chemical patterns for selective protein adhesion for high-density arrays that do not quench fluorescence.[30] Briefly, the developed areas of patterned PMMA on thermal oxide were first silanized with 0.5% octadecyltrichlorosilane (OTS, Aldrich) in carbon tetrachloride, which is a PMMA nonsolvent. The long alkyl chains of the OTS self-assembled monolayer (SAM) promote protein adhesion. After the PMMA was stripped in methylene chloride, the remaining unsilanized areas were passivated with 1% PEG-silane (Gelest) in tetrahydrofuran to prevent protein fouling or nonspecific adsorption. Figure 8 shows a confocal fluorescence image (Zeiss LSM Pascal) of immobilized Alexa-Fluor 546/streptavidin conjugate (Molecular Probes) in an array of 400 nm spots on a 2400 nm pitch after soaking for 1 h at room temperature (2 μg/mL in phosphate-buffered saline).

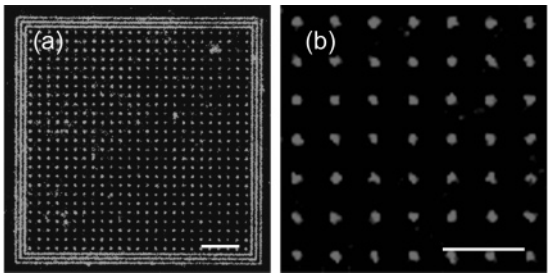

Figure 8. Confocal fluorescence image of an array of AlexaFluor-546/streptavidin conjugate with 400 nm spots on a 2.4 μm pitch. A binary chemical pattern for selective protein adhesion was created by first modifying the developed areas of patterned PMMA on thermal oxide with octadecyltrichlorosilane to promote protein adhesion, and then PEG-silane after stripping the resist to prevent nonspecific adorption. (a) Scale bar = 10 μm. (b) Scale bar = 5 μm.

While all results presented in this Letter were for 65 nm PMMA on glass or thermal oxide, the values reported here are not universal, and there are several material considerations for CE-EBL. First, the thickness of the resist must be less than the penetration depth of the beam or Kanaya−Okayama range (R_{KO})[31]

$$R_{KO} = 0.0276AE_0^{1.67}/Z^{0.89}d \quad (3)$$

where A is the atomic weight (g/mol), E_0 is the incident beam energy (keV), Z is the atomic number, and d is the density (g/mL). Second, E_2 of the resist varies with the thickness and material properties of both the resist and the substrate. Last, the maximum resist thickness may be limited if a single resist layer is used. For example, a thick PMMA layer cannot be patterned on glass by CE-EBL because the energy required to penetrate the resist will invariably be larger than E_2 and charge the resist-on-insulator.

In conclusion, we have demonstrated the use of CE-EBL to pattern nanostructures on insulating substrates by adapting concepts of low-voltage scanning electron microscopy and lithography. The pattern distortion from surface charging was minimized by the precise control of the electron beam energy, eliminating the need for additional charge dissipation layers or sophisticated gas delivery systems. Sub-100 nm PMMA features on glass were easily fabricated at area and line doses as low as 10 μC/cm^2 and 0.125 nC/cm, respectively. This method of nanoscale patterning on insulators and wide band gap materials has potential applications in high-density biochips, flexible polymeric electronics, and optoelectronics.

Furthermore, the technique employed in CE-EBL of variable magnification scanning to find the critical voltage prior to exposure may improve resolution and fidelity in low-voltage e-beam lithography on all substrates for the development of parallel microarray columns.

Acknowledgment. This research was funded by DARPA (N66001-05-X-6030) and the Center for Bits and Atoms (NSF Grant Number CCR0122419). The authors thank Scott Manalis for generous use of his AFM, and Marc Gershow for helpful discussion. J.J. is on partial fellowship support of the Korea Foundation for Advanced Studies.

References

(1) Gross, B. In *Electrets*; Sessler, G. M., Ed.; Topics in applied phyiscs; Springer-Verlag: New York, 1980; Vol. 33, pp 230−252.
(2) Reimer, L.; Golla, U.; Bongeler, R.; Kassens, M.; Schindler, B.; Senkel, R. *Optik* **1992**, *92*, 14−22.
(3) Reimer, L. *Image formation in low-voltage scanning electron microscopy*; SPIE Optical Engineering Press: Bellingham, WA, 1993.
(4) Joy, D. C.; Joy, C. S. *Micron* **1996**, *27*, 247−263.
(5) Ong, C. K.; Song, Z. G.; Gong, H. *J. Phys.*: *Condens. Matter* **1997**, *9*, 9289.
(6) Satyalakshmi, K. M.; Olkhovets, A.; Metzler, M. G.; Harnett, C. K.; Tanenbaum, D. M.; Craighead, H. G. *J. Vac. Sci. Technol., B* **2000**, *18*, 3122−3125.
(7) Cummings, K. D. *J. Vac. Sci. Technol., B* **1990**, *8*, 1786−1788.
(8) Itoh, H.; Nakamura, K.; Hayakawa, H. *J. Vac. Sci. Technol., B* **1989**, *7*, 1532−1535.
(9) Liu, W.; Ingino, J.; Pease, R. F. *J. Vac. Sci. Technol., B* **1995**, *13*, 1979−1983.
(10) Bai, M.; Pease, R. F. W.; Tanasa, C.; McCord, M. A.; Pickard, D. S.; Meisburger, D. *J. Vac. Sci. Technol., B* **1999**, *17*, 2893−2896.
(11) Cumming, D. R. S.; Khandaker, I. I.; Thoms, S.; Casey, B. G. *J. Vac. Sci. Technol., B* **1997**, *15*, 2859−2863.
(12) Steingruber, R.; Ferstl, M.; Pilz, W. *Microelectron. Eng.* **2001**, *57*−*8*, 285−289.
(13) Dobisz, E. A.; Bass, R.; Brandow, S. L.; Chen, M. S.; Dressick, W. J. *Appl. Phys. Lett.* **2003**, *82*, 478−480.
(14) Angelopoulos, M.; Shaw, J. M.; Kaplan, R. D.; Perreault, S. *J. Vac. Sci. Technol., B* **1989**, *7*, 1519−1523.
(15) Angelopoulos, M. *IBM J. Res. Dev.* **2001**, *45*, 57−75.
(16) Hupcey, M. A. Z.; Ober, C. K. *J. Vac. Sci. Technol., B* **1998**, *16*, 3701−3704.
(17) Myers, B. D.; Dravid, V. P. *Nano Lett.* **2006**, *6*, 963−968.
(18) Danilatos, G. D. *Adv. Electron. Electron Phys.* **1988**, *71*, 109−250.
(19) Toth, M.; Phillips, M. R.; Thiel, B. L.; Donald, A. M. *J. Appl. Phys.* **2002**, *91*, 4479−4491.
(20) Durkin, R.; Shah, J. S. *J. Microsc. (Oxford, U.K.)* **1993**, *169*, 33−51.
(21) Thiel, B. L.; Toth, M. *J. Appl. Phys.* **2005**, *97*, 051101/1−051101/18.
(22) Butler, J. H.; Joy, D. C.; Bradley, G. F.; Krause, S. J. *Polymer* **1995**, *36*, 1781−1790.
(23) Mun, L. M.; Drouin, D.; Lavallee, E.; Beauvais, J. *Microsc. Microanal.* **2004**, *10*, 804−809.
(24) Peterson, P. A.; Radzimski, Z. J.; Schwalm, S. A.; Russell, P. E. *J. Vac. Sci. Technol., B* **1992**, *10*, 3088−3093.
(25) Olkhovets, A.; Craighead, H. G. *J. Vac. Sci. Technol., B* **1999**, *17*, 1366−1370.
(26) Lee, Y. H.; Browning, R.; Maluf, N.; Owen, G.; Pease, R. F. W. *J. Vac. Sci. Technol., B* **1992**, *10*, 3094−3098.
(27) Joy, D. C.; Joy, C. S. *Microsc. Microanal.* **1998**, *4*, 475−480.
(28) Legressus, C.; Valin, F.; Gautier, M.; Duraud, J. P.; Cazaux, J.; Okuzumi, H. *Scanning* **1990**, *12*, 203-210.
(29) Hovington, P.; Drouin, D.; Gauvin, R. *Scanning* **1997**, *19*, 1−14.
(30) Lussi, J. W.; Tang, C.; Kuenzi, P. A.; Staufer, U.; Csucs, G.; Voros, J.; Danuser, G.; Hubbell, J. A.; Textor, M. *Nanotechnology* **2005**, *16*, 1781−1786.
(31) Kanaya, K.; Okayama, S. *J. Phys. D*: *Appl. Phys.* **1972**, *5*, 43.

NL061211Q